Archival Report

Biological Psychiatry: CNNI

Manipulating Reward Sensitivity Using Reward Circuit–Targeted Transcranial Magnetic Stimulation

Jon Ryan, Jourdan J. Pouliot, Greg Hajcak, and Derek Evan Nee

ABSTRACT

BACKGROUND: The reward circuit is important for motivation and learning, and dysregulations of the reward circuit are prominent in anhedonic depression. Noninvasive interventions that can selectively target the reward circuit may hold promise for the treatment of anhedonia.

METHODS: We tested a novel transcranial magnetic stimulation intervention for modulating the reward circuit. A total of 35 healthy individuals participated in a crossover controlled study targeting the reward circuit or a control site with intermittent theta burst stimulation (iTBS), an excitatory form of transcranial magnetic stimulation. Individual reward circuit targets were defined based upon functional magnetic resonance imaging functional connectivity with the ventral striatum, yielding targets in the rostromedial prefrontal cortex (rmPFC). Reward circuit function was assessed at baseline using functional magnetic resonance imaging, and reward circuit modulation was assessed using an event-related potential referred to as the reward positivity, which has been shown to reliably track reward sensitivity, as well as individual differences in depression and risk for depression.

RESULTS: Relative to control iTBS, rmPFC iTBS enhanced the reward positivity. This effect was moderated by reward function, suggesting greater enhancements in individuals with lower reward function. This effect was also moderated by rmPFC–ventral striatum connectivity insofar as iTBS reached the rmPFC, suggesting that efficacy relies jointly on the strength of the rmPFC–ventral striatum pathway and ability of transcranial magnetic stimulation to target the rmPFC.

CONCLUSIONS: These data suggest that the reward circuit can be modulated by rmPFC iTBS, and amenability to such modulations is related to measures of reward circuit function. This provides the first step toward a novel noninvasive treatment of disorders of the reward circuit.

https://doi.org/10.1016/j.bpsc.2022.02.011

Depressive disorders are prevalent (1), causing substantial suffering, disability, and socioeconomic costs (2,3). A core characteristic of depression is anhedonia—the lack of interest or pleasure in typically enjoyable experiences—which is thought to arise from deficits in reward processing (4). Correspondingly, depression has been linked to reduced activation of the brain's mesolimbic reward system with functional magnetic resonance imaging (fMRI) meta-analyses converging on the ventral striatum (VS) as a consistent locus of hypoactivation (5–7). Normalizing such hypoactivity may therefore hold promise in the treatment of anhedonic depression. Progress toward this end requires 1) measures that reliably track reward circuit function and 2) interventions that modulate these measures.

Toward the former, reward dysfunction in depression has been documented using the reward positivity (RewP), a relative positivity in the event-related potential following rewards compared with nonrewards (8,9). The RewP correlates with behavioral (10) and fMRI measures of dopaminergic reward circuit function including VS activation (11,12). Individuals with depression are characterized by a reduced RewP (13–16). Moreover, a blunted RewP predicts increases in depression (17,18) and interacts with stressors to predict later increases in depressive symptoms (19). The RewP also predicts successful treatment response to interventions for depression (20–22), as well as the course of depression (23). Collectively, these data suggest that the RewP tracks reward circuit (dys)function and could be a novel target for intervention and prevention efforts.

Transcranial magnetic stimulation (TMS) is a promising tool for modulating brain function. However, reward structures (e.g., the VS) cannot be targeted directly by TMS owing to their deep location. Nevertheless, a growing body of research has demonstrated that TMS to cortical areas can indirectly modulate neuroanatomically connected subcortical areas (24,25) with evidence that TMS to frontal areas modulates the dorsal striatum (26,27). Given that the VS is neuroanatomically connected to the rostromedial prefrontal cortex (rmPFC) (28–30), TMS to the rmPFC may modulate the VS and reward circuit function (Supplement).

ISSN: 2451-9022

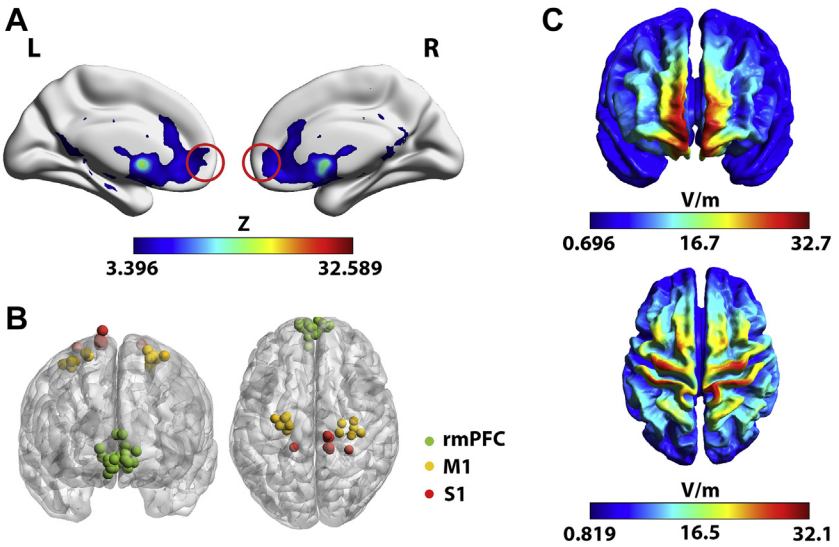

Figure 1. Functional connectivity and transcranial magnetic stimulation targeting. **(A)** Group level map of functional connectivity with the ventral striatum. **(B)** Individualized connectivity was used to determine participant-specific transcranial magnetic stimulation targeting within the rostromedial prefrontal cortex (rmPFC). Experimental targets were chosen within superficial areas of high connectivity. Spheres indicate individualized rmPFC experimental targets (green) and the primary motor cortex (M1)/primary somatosensory cortex (S1) control targets (orange/red). Experimental and control targets within participants were administered to the same hemisphere. **(C)** Group-level maps of the simulated e-fields (norm E) during stimulation of the experimental (top) and control (bottom) targets. L, left; R, right.

Here, we tested the hypothesis that TMS to the rmPFC modulates reward circuit function as reflected by the RewP. We used intermittent theta burst stimulation (iTBS), an excitatory form of TMS designed to upregulate neural activity (31). Relative to iTBS delivered to a control target, we hypothesized that rmPFC iTBS targeting the reward circuit would increase the RewP (Figure 1). Moreover, we examined whether rmPFC iTBS modulation of the RewP is moderated by reward circuit function and rmPFC-VS connectivity. We predicted that individuals with reward circuit hypoactivity may benefit the most from rmPFC iTBS and that the strength of rmPFC-VS connectivity may enhance propagation of TMS signals through the reward circuit, resulting in greater rmPFC iTBS modulations of the RewP.

METHODS AND MATERIALS

Participants

A total of 35 right-handed participants (age 18–26 years; mean = 20 years; *n* = 24 female) without contraindications for fMRI and TMS and no self-reported history of neurologic or psychiatric disorders were recruited from the Tallahassee, Florida, area. Planned recruitment (*N* = 40) was truncated by COVID-19. Exclusions (Supplement) left 24 participants for iTBS/electroencephalography (EEG) analyses, 30 for fMRI analyses, and 23 for analyses combining iTBS/EEG and fMRI.

Procedure

Participants performed three sessions. A baseline session included MRI scanning and TMS motor thresholding. iTBS/EEG sessions followed within 10 days and were spaced 1 week apart from one another (8 days for 1 participant). Each iTBS session consisted of iTBS to either the rmPFC or control target (see below) followed immediately by the Doors task with EEG recording. The order of stimulation targets was randomly counterbalanced across participants. This study was approved by the Institutional Review Board at Florida State University (IRB Nos. STUDY00000532, STUDY00000533, and STUDY00000973).

Tasks

The Doors task (Figure 2A) was designed to engage the reward circuit (8). On each trial, two identical doors were presented on a computer screen. Participants were told that they would either win or lose money on each trial and to guess which door would result in monetary gain. Because monetary losses are experienced as twice as valuable as monetary gains (32), participants were told that they could either win $0.50 or lose $0.25 on each trial and that they would get to keep their winnings. The task consists of 30 gain trials and 30 loss trials, presented in pseudorandom order such that participant choices had no actual bearing upon outcomes. The task was administered using Presentation (Neurobehavioral Systems, Inc.) for the EEG version and E-Prime (Psychology Software Tools) for the fMRI version.

For the EEG version, participants were shown a fixation cross (500 ms) followed by an image of two doors, which remained until participants made a selection by clicking either the left or right mouse button. After another fixation cross (interstimulus interval: 1000 ms), feedback indicating monetary gain (green upward arrow) or loss (red downward arrow) was presented (2000 ms). Finally, a fixation cross (intertrial interval) was presented for 1500 ms, followed by the message “Click For Next Round,” which remained until the participant clicked a mouse button. The fMRI version had different timing to account for hemodynamic lag and used finger presses for responding: doors were presented for a fixed time of 4000 ms, the interstimulus interval was uniformly pseudorandomized between 2000 and 5000 ms in 1000-ms increments, and the intertrial interval was pseudorandomized between 1500 and 9000 ms in 2500-ms increments in a weighted fashion (24 trials at 1500 ms, 16 trials at 4000 ms, 12 trials at 6500 ms, 8 trials at 9000 ms).

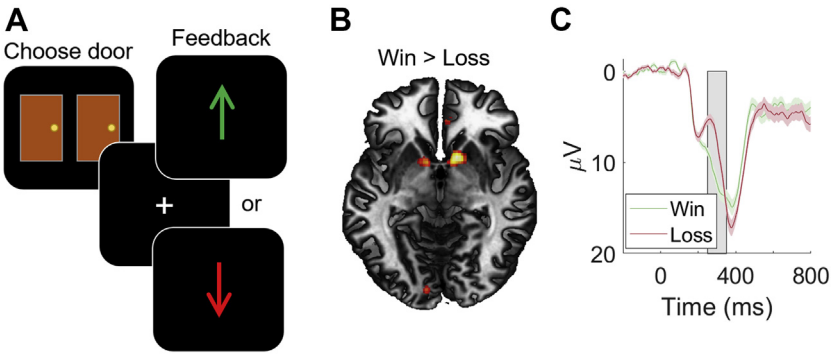

Figure 2. **(A)** Doors task. Participants selected a door and randomly received win (green arrow) or loss (red arrow) feedback, which was translated to monetary compensation. **(B)** Functional magnetic resonance imaging activation for win > loss feedback. Results are visualized at T > 5. **(C)** Event-related potentials after win and loss feedback in the control–intermittent theta burst stimulation session. Positive is plotted down. Time window of interest is highlighted in gray. The reward positivity is reflected by the more positive going potential for wins (green) relative to losses (red).

Prior to performing the Doors task in the scanner, participants completed a 9-minute eyes open resting-state scan while maintaining fixation.

EEG Recording

EEG was recorded using an elastic cap with 10 actiCAP slim electrodes positioned in accordance with the 10/20 system using a LiveAmp amplifier (Brain Products GmbH). Electrode FCz served as an online recording reference, with a ground electrode placed at FPz. Two electrodes were placed on the left (TP9) and right (TP10) mastoids. Electro-oculogram was recorded using four electrodes: two placed approximately 1 cm above and below the left eye and two at the outer canthi of both eyes. The remaining two electrodes were placed at Cz and Pz. The EEG signal was digitized at 500 Hz. Impedance was kept below 25 kΩ.

EEG Processing

EEG data were analyzed using BrainVision Analyzer, version 2.1 (Brain Products GmbH). Data were re-referenced offline to the average of the left and right mastoids and bandpass filtered (0.1–30 Hz). Data were segmented into feedback-locked epochs from −200 to 1000 ms, with −200 to 0 ms serving as the baseline. Ocular artifacts were corrected (33). Epochs containing a voltage step >50 μV between consecutive sample points, a 175-μV change within a 400-ms interval, or a change of <0.5 μV within a 100-ms interval were automatically rejected. Feedback event-related potentials were then averaged separately for win and loss trials.

The RewP was initially assessed by contrasting the average signal between 250 and 350 ms at FCz following win and loss feedback as we have done previously (8,14). While this method offers an unbiased assessment of the difference between win and loss feedback, a windowed average may obscure the contributions of multiple components (34). To more precisely quantify the RewP, we used the peak positivity in the win minus loss difference waveform between 200 and 400 ms at FCz, following (35) and recommended by a RewP meta-analysis (34). This measure of the RewP was made separately for each visit and was used in subsequent analyses.

Image Acquisition

MRI data were acquired on a Siemens Prisma 3T scanner equipped with a 32-channel head coil. A high-resolution T1 structural MRI (magnetization-prepared rapid acquisition gradient-echo; 384 × 384 × 256 matrix of 0.67 × 0.67 × 0.7 mm^3 voxels; repetition time = 1.84 seconds; echo time = 2.9 ms; flip angle = 9) was collected along with a T2 (256 × 256 × 192 matrix of 0.9 mm^3 isotropic voxels; repetition time = 3.2 seconds; echo time = 408 ms). T2*-weighted echo-planar imaging images were collected during the Doors task and resting state described below (84 × 84 × 54 matrix of 2.5 mm^3 isotropic voxels; repetition time = 2 seconds; multiband = 2; echo time = 29.2 ms; flip angle = 45).

Univariate Image Analysis

SPM12 (https://www.fil.ion.ucl.ac.uk/spm/software/spm12/) was used for preprocessing and analysis unless specified otherwise. Images were converted from DICOM into NIfTI format. Origins for all images were manually set to the anterior commissure. Functional data were spike corrected using AFNI's 3dDespike (http://afni.nimh.nih.gov/afni). Functional images were corrected for differences in slice timing using sinc-interpolation and head movement using a least squares approach and a six-parameter rigid body spatial transformation. Structural data were coregistered to the functional data and segmented into gray and white matter probability maps (36). Segmented images were used to calculate spatial normalization parameters to the Montreal Neurological Institute template, which were applied to the functional data. As part of spatial normalization, the data were resampled to 2 × 2 × 2 mm^3. Functional images were isotropically Gaussian smoothed at 8-mm full width at half maximum. All analyses included a temporal high-pass filter (128 seconds) and an autoregressive AR(1) model to correct temporal autocorrelation, and images were runwise scaled to a global mean intensity of 100.

Subject-level models were fit with a general linear model including separate regressors capturing win feedback, loss feedback, left responses, right responses, and visual presentation of the doors. Each model also included linear motion parameters as well as framewise displacement to capture motion-related signals.

A win minus loss contrast was performed at the subject level and submitted to a second-level one-sample t test thresholded with a $p < .001$ height and 402 voxel extent to achieve familywise error cluster-corrected $p < .05$. To produce covariates for correlation and moderation analyses, 6-mm spherical regions of interest were centered at peaks of activation in the dataset in the left (−12, 6, −6) and right (16, 8, −8) VS and medial PFC (−10, 52, 0). Region of interest activations were used to correlate with the statistically independent RewP. The blood oxygen level–dependent signal is affected by magnetic field inhomogeneities and head motion. To remove these artifactual contributions, for each region of interest, temporal signal-to-noise ratio (mean divided by standard deviation) and head motion [root mean square of framewise displacement (37)] were regressed out. The resultant residuals were used as variates to correlate with the RewP (analyses remain qualitatively unchanged using the original, non-residualized contrasts).

Connectivity Analysis and iTBS Targeting

Following Parkes *et al.* (38), we modified preprocessing to calculate connectivity: ANTs toolbox (http://stnava.github.io/ANTs/) was used for T1 N4 bias field correction and spatial normalization to the Montreal Neurological Institute template. The first four volumes of each functional scan were discarded to ensure MRI gradient stabilization. Montreal Neurological Institute tissue masks were generated for noise correction using fslmaths (https://fsl.fmrib.ox.ac.uk/fsl/fslwiki/FSL). Intensity normalization was conducted on brain-masked functional data, followed by linear detrending of the functional images using the REST toolkit (https://www.nitrc.org/projects/rest/). We applied 6-mm full width at half maximum isotropic Gaussian smoothing using SPM to all functional images, and frequencies below 0.008 Hz and above 0.08 Hz were filtered. ICA-AROMA (39)—with original white matter, cerebrospinal fluid signals (2Phys), and global signal regression—removed artifacts from head motion and other sources.

rmPFC targets were based upon individual functional connectivity. Following analogous prior work (40), we defined an rmPFC search space using group-averaged resting-state connectivity with the bilateral VS of an independent sample (n = 34) described previously (41,42). The VS was defined by resampling a high-resolution probabilistic atlas of the nucleus accumbens (43) to match the resolution of our preprocessed functional data. Voxelwise correlation maps with the VS were computed for each subject, transformed with an arc-hyperbolic tangent function, and submitted to a second-level one-sample t test. Significance was determined using voxel-level familywise error correction ($p < .05$) using SPM12. The rmPFC search space was defined by a 15-mm sphere around the rostral-most peak of connectivity with the VS (2, 56, −4). For each subject in this dataset, VS connectivity was similarly calculated, and connectivity maps and the rmPFC search space were inverse warped into native space. Individual connectivity maps were defined on either the rest (n = 11), task (n = 1), or combined (n = 12) data, wherein choice of dataset was determined by which connectivity map produced the greatest spatial similarity to the independent group-averaged map. An iTBS target was defined within the rmPFC search space using a manual procedure balancing maximal connectivity strength, minimal distance to scalp, and sufficient distance from the orbits so as to minimize discomfort.

To quantify individual connectivity with the VS, more rigorous procedures were used to facilitate merging of rest and task data. Systematic biases induced by task activations were removed from the task data using procedures described by Cole *et al.* (44). ICA-AROMA was then used to remove signal artifacts and roughly equate the variance of the rest and task data (Supplement). Rest and task data were then merged prior to computing functional connectivity. Group-averaged functional connectivity is depicted in Figure 1A.

A control iTBS target was localized to the hand-knob of the primary motor cortex (n = 15) or the dorsomedial-most tip of primary somatosensory cortex (n = 9) based upon visual inspection of the T1 image (Supplement). Control targets were matched to rmPFC targets in hemisphere. Targets are depicted in Figure 1B.

Simulated electrical fields (e-fields) were calculated using SimNIBS 2.1 software (45) (Figure 1C). E-field modeling indicated variability in how effectively iTBS reached our rmPFC targets. Therefore, we distinguished between the ideal target and the stimulated target. The ideal target was defined as the voxel within the rmPFC search space showing maximal connectivity with the VS for a given individual. The stimulated target was defined as the voxel within our rmPFC search space showing the maximum product of connectivity with the VS and norm E for a given individual. That is, the stimulated target weighs both connectivity and stimulation intensity. Individual connectivity averaged within a 6-mm sphere around the stimulated target was arc-hyperbolic tangent normalized and used for moderation analyses, along with the Euclidean distance between the stimulated target and ideal target.

TMS Procedures

TMS was delivered using a MagPro X100 stimulator equipped with a figure-of-eight MCF-B65 coil. Electromyography was recorded on the left dorsal interosseous muscle using a Delsys Trigno system and EMGworks Acquisition software (Delsys Inc.). A hunting procedure was used to determine the scalp location in the right hemisphere producing the maximal contralateral hand twitch at the minimal stimulation intensity. Next, the participant maintained voluntary contraction of the first dorsal interosseous muscle at approximately 20% of maximum contraction. Active motor threshold was determined as the minimal stimulation intensity needed to produce a motor evoked potential >50 μV in 5 of 10 pulses.

Following Huang *et al.* (31), iTBS was delivered in three pulse bursts at 50 Hz repeated at 5 Hz in 2-second trains repeated every 10 seconds at 80% of active motor threshold for a total of 600 pulses over 190 seconds. iTBS was guided using Localite hardware and software (Localite GmbH). For control iTBS, the coil was oriented perpendicular to the target gyrus. For rmPFC iTBS, the coil handle was oriented vertically toward the top of the participant's head to minimize stimulation around the orbits. Prior to the start of iTBS, a single test pulse

was delivered to the target at the same intensity of iTBS to acclimate the participant.

RESULTS

A contrast of win-loss in the fMRI data revealed significant reward-related activations in the bilateral VS and medial PFC (Figure 2B) consistent with previous reports (12,14,46). Correspondingly, following control iTBS, a robust RewP was observed such that more positive potentials were observed following wins relative to losses starting approximately 200 ms after feedback (mean difference between 250 and 350 ms = 3.4 μV; t_{23} = 3.31, p = .003) (Figure 2C). These data confirm the expected reward-related fMRI and EEG signals.

Previous data have indicated a relationship between VS fMRI activation and the RewP (11,12), suggesting that they reflect a common reward signal. Activation was also observed in the vicinity of our TMS targets, so we also examined the correspondence between medial PFC activation and the RewP (Supplement). Both the left (r = 0.32, p = .13) and right (r = 0.29, p = .18) VS showed a nonsignificant positive correlation with the RewP (Figure 3). While not significant, effect sizes were similar to prior data (12) (r = 0.30–0.34). However, reward-related activation in the medial PFC showed an opposite nonsignificant trend (r = −0.16, p = .46), which was significant when using robust regression to reduce the impact of an outlier (t_{21} = −2.43, p = .02). This negative relationship was striking given that medial PFC activations were positively correlated with the VS (left VS: r = 0.58, p = .003; right VS: r = 0.55, p = .007), suggesting that the RewP captures a signal more specifically related to the VS. After partialling out medial PFC activations, VS activation (averaged across hemispheres) was significantly positively correlated with the RewP (r = 0.51, p = .01). Robust regression verified that the positive relationship between VS activation and the RewP was not due to outliers (t_{20} = 2.23, p = .04). These data suggest that the VS and RewP reflect a common reward signal, consistent with prior data (11,12).

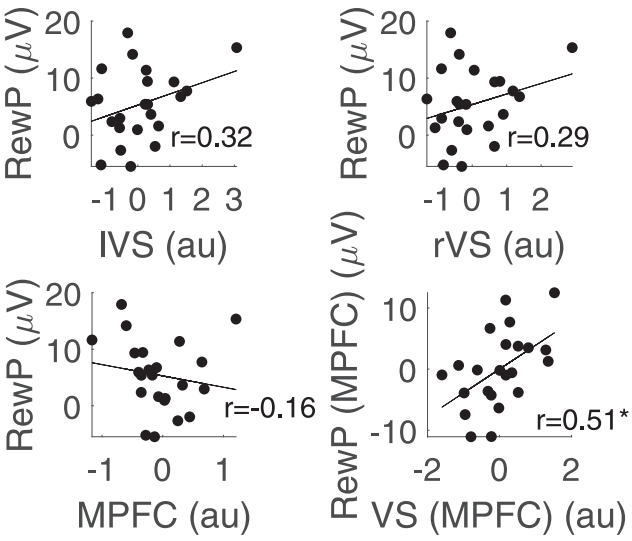

Figure 3. Correlations between the left ventral striatum (lVS), right VS (rVS), medial prefrontal cortex (MPFC), and the reward positivity (RewP). The RewP and VS were significantly positively correlated after controlling for the MPFC. *p < .05.

Next, we examined whether reward circuit–targeted iTBS modulates reward signaling. Following rmPFC iTBS, a significant RewP was observed (mean difference between 250 and 350 ms = 5.45 μV; t_{23} = 5.61, p < .00005). A mixed-effects analysis of variance with factors of feedback (win, loss), iTBS target (rmPFC, control), and iTBS order (rmPFC → control, control → rmPFC) revealed a trend toward a feedback × iTBS target interaction ($F_{1,22}$ = 3.87, p = .062) (Figure 4). This trend was driven by numerically larger responses to win feedback following rmPFC iTBS relative to control iTBS (mean difference = 2.9 μV; t_{23} = 2.03, p = .054) with no corresponding difference to loss feedback (mean difference = 0.1 μV; t_{23} = 0.09, p > .9). These data are suggestive of a selective effect of rmPFC iTBS to reward, but not loss signals. However, the lack of statistical significance suggests that the effect is not uniformly observed.

We tested two moderations of the rmPFC iTBS effect on reward processing. First, we examined whether those individuals with less reward signaling would show greater reward upregulation as a function of rmPFC iTBS. To do so, we created a latent variable reflecting reward signaling by combining left VS, right VS, and medial PFC reward-related activations (win-loss) and the RewP following control iTBS using principal component analysis (Supplement). We then correlated reward signaling with the change in RewP as a

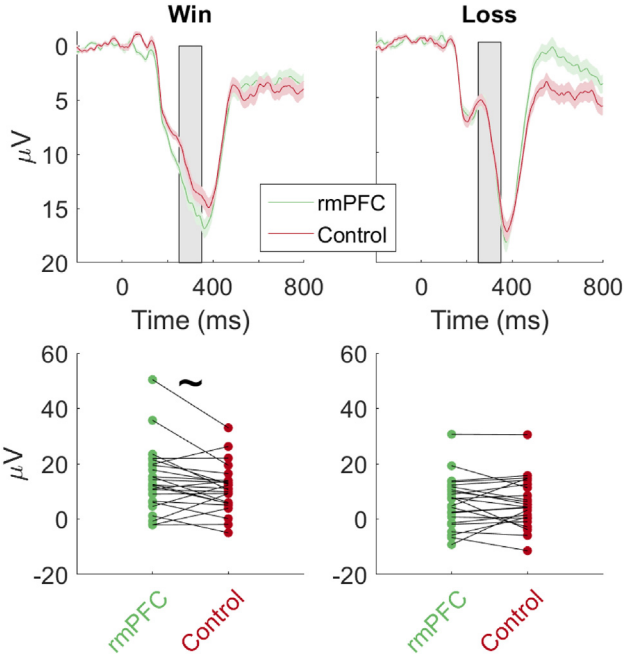

Figure 4. The reward positivity × transcranial magnetic stimulation target. (Top) More positive event-related potentials were observed in response to wins after rostromedial prefrontal cortex (rmPFC)–intermittent theta burst stimulation (iTBS) (green) compared with control iTBS (red). Losses showed no difference within the time period of interest. (Bottom) Win (left) and loss (right) event-related potentials summarized for each individual following rmPFC iTBS (green) and control iTBS (red). A trend was observed for a selective increase for wins following rmPFC iTBS.

function of rmPFC iTBS (rmPFC iTBS > control iTBS; ΔRewP). Consistent with the hypothesis, a significant linear negative relationship was observed ($r = -0.46$, $p = .03$) (Figure 5A), which held when using robust regression to reduce impact of potential outliers ($t_{21} = -2.61$, $p = .02$). Similar results were obtained when using fMRI activations alone as a moderator (Supplement). While those individuals with high reward signals (latent variable > 0) did not show an increase in the RewP following rmPFC iTBS (mean ΔRewP = −0.64 μV, $t_8 = -0.23$, $p = .81$), those with low reward signaling (latent variable < 0) did (mean ΔRewP = 4.01 μV, $t_{13} = 3.14$, $p = .008$) (Figure 5B). These data suggest that those individuals with low reward signaling are those who are specifically amenable to rmPFC iTBS.

Second, we tested the hypothesis that the effect of rmPFC iTBS is moderated by rmPFC-VS connectivity. Stronger rmPFC-VS connectivity should reflect a stronger pathway by which TMS can affect the reward circuit. However, this is qualified by the effectiveness with which TMS affects the rmPFC itself. To incorporate these two factors, we identified the stimulated target by weighing both the connectivity of the rmPFC to the VS and the e-field generated in the rmPFC (see Methods and Materials). The stimulated target differed from the ideal target—the rmPFC voxel showing maximal connectivity to the VS (mean distance = 16.7 mm, range = 0.66–31.3 mm). Although rmPFC-VS connectivity at the stimulated target was nonsignificantly positively related to the ΔRewP ($r = 0.35$, $p = .11$; robust regression $t_{21} = 1.62$, $p = .12$) (Figure 6A), this was qualified by a significant inverse relationship of the distance between the stimulated target and ideal target and the ΔRewP ($r = -0.49$, $p = .02$; robust regression $t_{21} = -2.42$, $p = .02$) (Figure 6B). This suggests that the effectiveness of rmPFC iTBS is related to the efficacy with which TMS can be directed to the ideal target for an individual. A component reflecting the shared variance among these measures (Supplement) was significantly correlated to the ΔRewP ($r = 0.47$, $p = .02$; robust regression $t_{21} = 2.29$, $p = .03$) (Figure 6C). These data suggest that effectiveness of rmPFC iTBS to increase the RewP is moderated jointly by the connectivity of the rmPFC to the VS and the efficacy with which TMS can reach the appropriate rmPFC target.

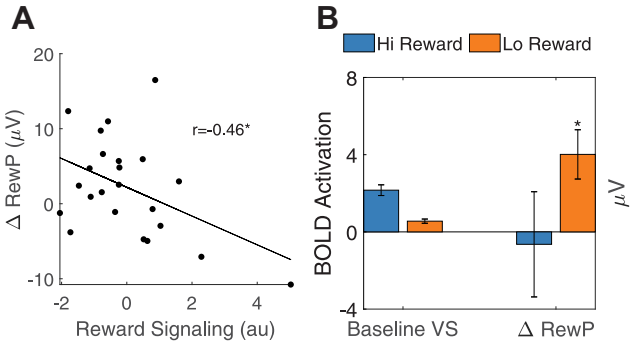

Figure 5. **(A)** Correlations among reward signaling and the change in reward positivity (RewP) from rostromedial prefrontal cortex intermittent theta burst stimulation relative to control intermittent theta burst stimulation (ΔRewP). **(B)** Left: ventral striatum (VS) reward-related activations in individuals with high (Hi) (blue) and low (Lo) (orange) reward signaling. Right: ΔRewP was significantly positive in low-, but not high-reward individuals. BOLD, blood oxygen level–dependent. *$p < .05$.

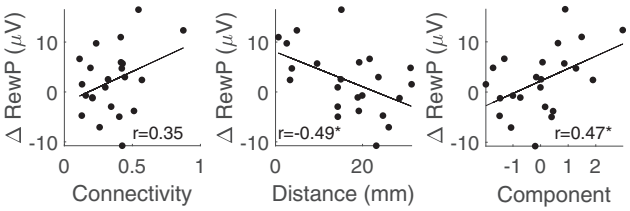

Figure 6. Moderation of rostromedial prefrontal cortex intermittent theta burst stimulation induced change in reward positivity (ΔRewP) by connectivity and transcranial magnetic stimulation efficacy. ΔRewP was nonsignificantly positively correlated with connectivity (arc-hyperbolic tangent normalized) at the stimulated target in rostromedial prefrontal cortex (left) and negatively correlated with the distance of the stimulated target from the ideal target (i.e., the area of maximum connectivity with the ventral striatum for an individual; middle). A component jointly reflecting connectivity and efficacy of transcranial magnetic stimulation to reach the ideal target was significantly related to the ΔRewP (right). *$p < .05$.

DISCUSSION

We tested a novel intervention targeting the reward circuit to modulate reward processing. By delivering iTBS to an rmPFC area showing functional connectivity to the VS, a critical node in the reward circuit, we found evidence of modulated reward processing reflected by increased RewP relative to control iTBS. This effect was selective to reward rather than loss feedback (Supplement) and was moderated by reward signaling. The increase in RewP induced by rmPFC iTBS was also related to rmPFC-VS connectivity insofar as TMS could reach the rmPFC. Collectively, these data provide evidence that rmPFC iTBS modulates reward processing, particularly in those individuals with low reward signaling and strong VS connectivity in areas that can be reached by TMS.

We tracked changes in reward processing using the RewP. Consistent with data reported here, a larger RewP has previously been related to increased structural (47) and functional (11,12,14) measures of the reward circuit obtained using MRI, as well as increased behavioral and self-report measures of reward sensitivity (10,48). Moreover, the RewP has clinical relevance because it is blunted in individuals with major depressive disorder (5,13,14,16,48–50), predicts risk for (17–19,51–54) and course of depression (15), and normalizes following successful treatment (55). The RewP's psychometric properties (56), low cost, and ease of obtainment make it a desirable general index of reward circuit function and target for interventions. The finding that rmPFC iTBS increases the RewP therefore holds promise for clinical interventions targeting the reward circuit.

TMS has been used for the treatment of drug-resistant depression. The most common treatment targets the dorsolateral PFC (57,58) with evidence that patients with different symptoms respond differentially to distinct dorsolateral PFC targets and corresponding circuits (36,59). Depressed individuals characterized by high levels of anhedonia have been among the most challenging to treat with TMS (60). An interesting future avenue would be to directly compare rmPFC and dorsolateral PFC TMS and contrast their effects on brain circuits and symptoms (see the Supplement).

Various limitations should be considered. First, the sample was truncated owing to COVID-19. Future studies using larger

samples will provide more definitive conclusions regarding the efficacy and effect sizes of rmPFC iTBS. Second, we sampled healthy individuals who were unselected for increased anhedonia. The extent to which the effects extend to psychiatric populations and the effects of rmPFC iTBS on anhedonia itself remain to be elucidated. However, the fact that those individuals with the lowest reward-related activations showed the greatest responsivity to rmPFC iTBS provides some promise for populations characterized by reward circuit hypofunction. Third, although we individualized rmPFC targeting based upon connectivity, our data indicate that both connectivity and e-fields dictate the effectiveness of rmPFC iTBS. While we anticipated the importance of individual connectivity based upon past work (24,40,61), the incorporation of e-fields was done post hoc. Our data suggest that incorporating e-field modeling to select targets may facilitate the effectiveness of interventions. However, the post hoc nature of the finding merits replication before reaching strong conclusions. Finally, our experimental and control targets likely differed in sensation. Discomfort from TMS is known to increase at more ventral areas relative to dorsal areas (62). Notably, the fact that the efficacy of rmPFC iTBS varied as a function of reward circuit factors (i.e., reward sensitivity, connectivity) suggests that the effect owes to the targeted network rather than reflecting a difference between TMS targets. Nevertheless, better control for discomfort would be prudent for future investigations.

We have provided evidence that a novel TMS intervention targeting the reward circuit modulates reward processing. This intervention may hold promise for the treatment of dysfunctions of the reward circuit.

ACKNOWLEDGMENTS AND DISCLOSURES

Portions of this study were funded by Florida State University Team Science for Translational Research Seed Grant, funded by the FSU Office of Research (DEN, GH).

Part of the results of the study were previously presented at the Southeast Regional Clinical & Translational Science Conference, March 2021, Emory University, Atlanta, Georgia, and Annual Meeting of the Society for Neuroscience, November 2021, Chicago, Illinois.

The authors report no biomedical financial interests or potential conflicts of interest.

ARTICLE INFORMATION

From the Departments of Biomedical Sciences (JR, GH) and Psychology (JR, GH, DEN), Florida State University, Tallahassee; and the Department of Psychology (JJP), University of Florida, Gainesville, Florida.

GH and DEN contributed equally to this work.

Address correspondence to Derek Evan Nee, Ph.D., at nee@psy.fsu.edu.

Received Dec 18, 2021; revised Feb 6, 2022; accepted Feb 23, 2022.

Supplementary material cited in this article is available online at https://doi.org/10.1016/j.bpsc.2022.02.011.

REFERENCES

1. Kessler RC, Bromet EJ (2013): The epidemiology of depression across cultures. Annu Rev Public Health 34:119–138.
2. Greenberg PE, Fournier AA, Sisitsky T, Simes M, Berman R, Koenigsberg SH, Kessler RC (2021): The economic burden of adults with major depressive disorder in the United States (2010 and 2018). Pharmacoeconomics 39:653–665.
3. Whiteford HA, Degenhardt L, Rehm J, Baxter AJ, Ferrari AJ, Erskine HE, *et al.* (2013): Global burden of disease attributable to mental and substance use disorders: Findings from the Global Burden of Disease Study 2010. Lancet 382:1575–1586.
4. Pizzagalli DA (2014): Depression, stress, and anhedonia: Toward a synthesis and integrated model. Annu Rev Clin Psychol 10:393–423.
5. Keren H, O'Callaghan G, Vidal-Ribas P, Buzzell GA, Brotman MA, Leibenluft E, *et al.* (2018): Reward processing in depression: A conceptual and meta-analytic review across fMRI and EEG studies. Am J Psychiatry 175:1111–1120.
6. Ng TH, Alloy LB, Smith DV (2019): Meta-analysis of reward processing in major depressive disorder reveals distinct abnormalities within the reward circuit. Transl Psychiatry 9:293.
7. Zhang WN, Chang SH, Guo LY, Zhang KL, Wang J (2013): The neural correlates of reward-related processing in major depressive disorder: A meta-analysis of functional magnetic resonance imaging studies. J Affect Disord 151:531–539.
8. Proudfit GH (2015): The reward positivity: From basic research on reward to a biomarker for depression. Psychophysiology 52:449–459.
9. Foti D, Novak KD, Hill KE, Oumeziane BA (2018): Neurophysiological assessment of anhedonia in depression and schizophrenia. In: Neurobiology of Abnormal Emotion and Motivated Behaviors. Amsterdam, the Netherlands: Elsevier, 242–256.
10. Bress JN, Hajcak G (2013): Self-report and behavioral measures of reward sensitivity predict the feedback negativity. Psychophysiology 50:610–616.
11. Becker MP, Nitsch AM, Miltner WH, Straube T (2014): A single-trial estimation of the feedback-related negativity and its relation to BOLD responses in a time-estimation task. J Neurosci 34:3005–3012.
12. Carlson JM, Foti D, Mujica-Parodi LR, Harmon-Jones E, Hajcak G (2011): Ventral striatal and medial prefrontal BOLD activation is correlated with reward-related electrocortical activity: A combined ERP and fMRI study. Neuroimage 57:1608–1616.
13. Brush CJ, Ehmann PJ, Hajcak G, Selby EA, Alderman BL (2018): Using multilevel modeling to examine blunted neural responses to reward in major depression. Biol Psychiatry Cogn Neurosci Neuroimaging 3:1032–1039.
14. Foti D, Carlson JM, Sauder CL, Proudfit GH (2014): Reward dysfunction in major depression: Multimodal neuroimaging evidence for refining the melancholic phenotype. Neuroimage 101:50–58.
15. Klawohn J, Burani K, Bruchnak A, Santopetro N, Hajcak G (2021): Reduced neural response to reward and pleasant pictures independently relate to depression. Psychol Med 51:741–749.
16. Liu WH, Wang LZ, Shang HR, Shen Y, Li Z, Cheung EF, Chan RC (2014): The influence of anhedonia on feedback negativity in major depressive disorder. Neuropsychologia 53:213–220.
17. Kujawa A, Proudfit GH, Klein DN (2014): Neural reactivity to rewards and losses in offspring of mothers and fathers with histories of depressive and anxiety disorders. J Abnorm Psychol 123:287–297.
18. Nelson BD, Perlman G, Klein DN, Kotov R, Hajcak G (2016): Blunted neural response to rewards as a prospective predictor of the development of depression in adolescent girls. Am J Psychiatry 173:1223–1230.
19. Burani K, Klawohn J, Levinson AR, Klein DN, Nelson BD, Hajcak G (2021): Neural response to rewards, stress and sleep interact to prospectively predict depressive symptoms in adolescent girls. J Clin Child Adolesc Psychol 50:131–140.
20. Brush CJ, Hajcak G, Bocchine AJ, Ude AA, Muniz KM, Foti D, Alderman BL (2022): A randomized trial of aerobic exercise for major depression: Examining neural indicators of reward and cognitive control as predictors and treatment targets. Psychol Med 52:893–903.
21. Burkhouse KL, Gorka SM, Klumpp H, Kennedy AE, Karich S, Francis J, *et al.* (2018): Neural responsiveness to reward as an index of depressive symptom change following cognitive-behavioral therapy and SSRI treatment. J Clin Psychiatry 79:17m11836.
22. Kujawa A, Burkhouse KL, Karich SR, Fitzgerald KD, Monk CS, Phan KL (2019): Reduced reward responsiveness predicts change in depressive symptoms in anxious children and adolescents following treatment. J Child Adolesc Psychopharmacol 29:378–385.
23. Klawohn J, Brush CJ, Hajcak G (2021): Neural responses to reward and pleasant pictures prospectively predict remission from depression. J Abnorm Psychol 130:702–712.

24. Wang JX, Rogers LM, Gross EZ, Ryals AJ, Dokucu ME, Brandstatt KL, *et al.* (2014): Targeted enhancement of cortical-hippocampal brain networks and associative memory. Science 345:1054–1057.
25. Hermiller MS, Chen YF, Parrish TB, Voss JL (2020): Evidence for immediate enhancement of hippocampal memory encoding by network-targeted theta-burst stimulation during concurrent fMRI. J Neurosci 40:7155–7168.
26. Strafella AP, Paus T, Barrett J, Dagher A (2001): Repetitive transcranial magnetic stimulation of the human prefrontal cortex induces dopamine release in the caudate nucleus. J Neurosci 21:RC157.
27. Strafella AP, Paus T, Fraraccio M, Dagher A (2003): Striatal dopamine release induced by repetitive transcranial magnetic stimulation of the human motor cortex. Brain 126:2609–2615.
28. Haber SN (2003): The primate basal ganglia: Parallel and integrative networks. J Chem Neuroanat 26:317–330.
29. Draganski B, Kherif F, Klöppel S, Cook PA, Alexander DC, Parker GJ, *et al.* (2008): Evidence for segregated and integrative connectivity patterns in the human Basal Ganglia. J Neurosci 28:7143–7152.
30. Gordon EM, Laumann TO, Marek S, Newbold DJ, Hampton JM, Seider NA, *et al.* (2021): Human fronto-striatal connectivity is organized into discrete functional subnetworks. bioRxiv. https://doi.org/10.1101/2021.04.12.439415.
31. Huang YZ, Edwards MJ, Rounis E, Bhatia KP, Rothwell JC (2005): Theta burst stimulation of the human motor cortex. Neuron 45:201–206.
32. Tversky A, Kahneman D (1992): Advances in prospect theory: Cumulative representation of uncertainty. J Risk Uncertainty 5:297–323.
33. Gratton G, Coles MG, Donchin E (1983): A new method for off-line removal of ocular artifact. Electroencephalogr Clin Neurophysiol 55:468–484.
34. Sambrook TD, Goslin J (2015): A neural reward prediction error revealed by a meta-analysis of ERPs using great grand averages. Psychol Bull 141:213–235.
35. Baker TE, Lesperance P, Tucholka A, Potvin S, Larcher K, Zhang YU, *et al.* (2017): Reversing the atypical valuation of drug and nondrug rewards in smokers using multimodal neuroimaging. Biol Psychiatry 82:819–827.
36. Fitzgerald PB (2021): Targeting repetitive transcranial magnetic stimulation in depression: Do we really know what we are stimulating and how best to do it? Brain Stimul 14:730–736.
37. Power JD, Barnes KA, Snyder AZ, Schlaggar BL, Petersen SE (2012): Spurious but systematic correlations in functional connectivity MRI networks arise from subject motion. Neuroimage 59:2142–2154.
38. Parkes L, Fulcher B, Yücel M, Fornito A (2018): An evaluation of the efficacy, reliability, and sensitivity of motion correction strategies for resting-state functional MRI. Neuroimage 171:415–436.
39. Pruim RHR, Mennes M, van Rooij D, Llera A, Buitelaar JK, Beckmann CF (2015): ICA-AROMA: A robust ICA-based strategy for removing motion artifacts from fMRI data. Neuroimage 112:267–277.
40. Tambini A, Nee DE, D'Esposito M (2018): Hippocampal-targeted theta-burst stimulation enhances associative memory formation. J Cogn Neurosci 30:1452–1472.
41. Nee DE, D'Esposito M (2016): The hierarchical organization of the lateral prefrontal cortex. Elife 5:e12112.
42. Nee DE, D'Esposito M (2017): Causal evidence for lateral prefrontal cortex dynamics supporting cognitive control. Elife 6:e28040.
43. Pauli WM, Nili AN, Tyszka JM (2018): A high-resolution probabilistic in vivo atlas of human subcortical brain nuclei. Sci Data 5:180063.
44. Cole MW, Ito T, Schultz D, Mill R, Chen R, Cocuzza C (2019): Task activations produce spurious but systematic inflation of task functional connectivity estimates. Neuroimage 189:1–18.
45. Saturnino GB, Puonti O, Nielsen JD, Antonenko D, Madsen KH, Thielscher A, *et al.* (2019): SimNIBS 2.1: A comprehensive pipeline for individualized electric field modelling for transcranial brain stimulation. In: Brain and Human Body Modeling: Computational Human Modeling at EMBC 2018. Cham, Switzerland: Springer, 3–25.
46. Foell J, Klawohn J, Bruchnak A, Brush CJ, Patrick CJ, Hajcak G (2021): Ventral striatal activation during reward differs between major depression with and without impaired mood reactivity. Psychiatry Res Neuroimaging 313:111298.
47. Carlson JM, Foti D, Harmon-Jones E, Proudfit GH (2015): Midbrain volume predicts fMRI and ERP measures of reward reactivity. Brain Struct Funct 220:1861–1866.
48. Bowyer CB, Joyner KJ, Yancey JR, Venables NC, Hajcak G, Patrick CJ (2019): Toward a neurobehavioral trait conceptualization of depression proneness. Psychophysiology 56:e13367.
49. Mulligan EM, Flynn H, Hajcak G (2019): Neural response to reward and psychosocial risk factors independently predict antenatal depressive symptoms. Biol Psychol 147:107622.
50. Belden AC, Irvin K, Hajcak G, Kappenman ES, Kelly D, Karlow S, *et al.* (2016): Neural correlates of reward processing in depressed and healthy preschool-age children. J Am Acad Child Adolesc Psychiatry 55:1081–1089.
51. Foti D, Kotov R, Klein DN, Hajcak G (2011): Abnormal neural sensitivity to monetary gains versus losses among adolescents at risk for depression. J Abnorm Child Psychol 39:913–924.
52. Weinberg A, Liu H, Hajcak G, Shankman SA (2015): Blunted neural response to rewards as a vulnerability factor for depression: Results from a family study. J Abnorm Psychol 124:878–889.
53. Bress JN, Smith E, Foti D, Klein DN, Hajcak G (2012): Neural response to reward and depressive symptoms in late childhood to early adolescence. Biol Psychol 89:156–162.
54. Hausman EM, Kotov R, Perlman G, Hajcak G, Kessel EM, Klein DN (2018): Prospective predictors of first-onset depressive disorders in adolescent females with anxiety disorders. J Affect Disord 235:176–183.
55. Barch DM, Whalen D, Gilbert K, Kelly D, Kappenman ES, Hajcak G, Luby JL (2019): Neural indicators of anhedonia: Predictors and mechanisms of treatment change in a randomized clinical trial in early childhood depression. Biol Psychiatry 85:863–871.
56. Levinson AR, Speed BC, Infantolino ZP, Hajcak G (2017): Reliability of the electrocortical response to gains and losses in the doors task. Psychophysiology 54:601–607.
57. George MS, Wassermann EM, Williams WA, Callahan A, Ketter TA, Basser P, *et al.* (1995): Daily repetitive transcranial magnetic stimulation (rTMS) improves mood in depression. Neuroreport 6:1853–1856.
58. Pascual-Leone A, Rubio B, Pallardó F, Catalá MD (1996): Rapid-rate transcranial magnetic stimulation of left dorsolateral prefrontal cortex in drug-resistant depression. Lancet 348:233–237.
59. Siddiqi SH, Taylor SF, Cooke D, Pascual-Leone A, George MS, Fox MD (2020): Distinct symptom-specific treatment targets for circuit-based neuromodulation. Am J Psychiatry 177:435–446.
60. Downar J, Geraci J, Salomons TV, Dunlop K, Wheeler S, McAndrews MP, *et al.* (2014): Anhedonia and reward-circuit connectivity distinguish nonresponders from responders to dorsomedial prefrontal repetitive transcranial magnetic stimulation in major depression. Biol Psychiatry 76:176–185.
61. Fox MD, Buckner RL, White MP, Greicius MD, Pascual-Leone A (2012): Efficacy of transcranial magnetic stimulation targets for depression is related to intrinsic functional connectivity with the subgenual cingulate. Biol Psychiatry 72:595–603.
62. Meteyard L, Holmes NP (2018): TMS SMART - Scalp mapping of annoyance ratings and twitches caused by transcranial magnetic stimulation. J Neurosci Methods 299:34–44.